Universe Scientific Publishing

Food Nutrition Chemistry 2024, 2(2), 154
https://doi.org/10.18686/fnc.v2i2.154

Article

Role of charge exchange collision on generation of active species for cold plasma food processing

M. Perumal[1,*], A. Saravanan[2], B. Muthukumar[1], Suraj Kumar Sinha[1]

[1] Department of Physics, Pondicherry University, Pondicherry 605014, India
[2] Sikkim Manipal Institute of Technology, Sikkim 737136, India
*** Corresponding authors:** M. Perumal, perumalphy@gmail.com

CITATION

Perumal M, Saravanan A, Muthukumar B, Sinha SK. Role of charge exchange collision on generation of active species for cold plasma food processing. Food Nutrition Chemistry. 2024; 2(2): 154. https://doi.org/10.18686/fnc.v2i2.154

ARTICLE INFO

Received: 3 April 2024
Accepted: 12 June 2024
Available online: 28 June 2024

Abstract: Charge exchange collision (CXC) is well known in solar and space plasmas. In this work, we present how the CXC between N_2^+ and N_2 can be exploited to overcome major challenges in cold plasma food processing (CPFP). CPFP is an emerging application of glow discharge plasmas for physicochemical modifications to achieve shelf-life enhancement, preservation, surface activation for germination, antimicrobial treatment, surface cleaning, etc. The commercial application of CPFP is in its infancy and it faces two major challenges. The first challenge is the difficulty in generating the desired active species for the required modification, and the second is the very high processing cost. In this paper, with the help of numerical modeling for nitrogen discharge, we show that the CXC between N_2^+ and N_2 can be utilized to generate active species selectively, enhance energy efficiency, and possibly eliminate the processing gas cost. The modeling is followed by experimental demonstration and validation of the proposed concept. This work may lead to a new direction of transdisciplinary research towards the commercial application of CPFP.

Keywords: glow discharge plasma; food processing; charge exchange collisions; high energy efficiency and plasma processing

1. Introduction

Cold plasma offers a chemical-free process and is one of the most promising food processing methods [1–5] among newly emerging techniques of food preservation and food safety [6–12]. Three mechanisms dominate in plasma treatment: i) physical damage to membranes and internal cellular components due to the bombardment of energetic species, ii) chemical reactions led by ions and radicals [3], and iii) radiation-induced damage [13–15]. These three governing processes dominate in various methods of cold plasma food processing (CPFP) reported for the treatment of meat [14,16], poultry [14], milk [14,17], water [17], cereals [14], fruits [16], and vegetables [14,17], as well as non-food processing, using atmospheric pressure plasma [18], cold atmospheric gas-phase plasma [19], RF plasma [20], microwave plasma [21], DC glow discharge [22], gliding arc discharge [23], dielectric barrier discharge [24], pulsed plasma [25], corona discharge [26], etc. Accordingly, an intense investigation is required to understand the mode of action of energetic species [5,12], radicals [3], reactive atomic species [6], and charged particles [12], as well as the radiation [3,12], feed gas [3], applied power, energy efficacy [2], and cost-effectiveness [3], of cold plasma food processing.

CPFP's diverse application and a wide range of plasma sources give rise to a multitude of unknown parameters. Therefore, our approach was to simplify this complexity. We focused on the classification of all possible types of active species

required for a specific modification in CPFP. From the review of reported works on CPFP, it was ascertained that mainly three categories of species are required. The details are given in the following Section 2. In Section 3, the fundamental mechanism of active species generation in cold plasma is discussed. In Section 4, we introduce how the charge exchange collision between N_2^+ and N_2 may be utilized for the selective extraction of active species for CPFP, followed by an experimental demonstration of a proposed method of food processing, and in the last section, we summarize the future perspective of CPFP.

2. Active species in cold plasma food processing

In the last decade, a large number of works on CPFP have been reported. A detailed review of most of the significant works in CPFP was conducted for different samples and various plasma sources [6–27]. A detailed list of reported species in cold plasma food processing is given in **Table 1**. Three types of main active species were identified for all desired modifications using CPFP. These main active species are:

i) Energetic ions with specific energy: for physicochemical modification.
ii) Excited species and radicals: for chemical modification, including microbial deactivation and surface cleaning.
iii) Radiations: for chemical modification and microbial deactivation.

We introduced a fourth type, called energetic neutrals, which has been usually ignored. Though neutral beam heating is one of the most important techniques of plasma heating in fusion plasma, its role in other plasma-based technologies is considered unimportant.

Table 1. Classification of CPFP on basis of modification required and corresponding active species.

Modification	Active species	Discharge type	Ref.
Physical damage to membranes and internal cellular components due to bombardment of energetic species, mainly ions	Ar^+, He^+, Ne^+, N_2^+	DC glow discharge	[7,8]
Chemical reactions led by chemically active species, such as electrons, ions, atoms and radicals, for chemical modification including microbial deactivation	ROS, RNS, NO_3^-, NO_2^-, H_2O_2, NO, NO_2, OH, HNO_3, O_3, NO_x, O, O_2, CN, N_2, N_2^+	DBD discharge	[24]
	O, OH, HO_2, O_3	Corona discharge	[26]
	O_3, O^-, NO, N_2, N_2^+, CO, O_2^+, OH, ROS, RNS, CO_2, HO, H_2O, SO_x, ions, electrons	RF discharge	[20]
	NO, OH, N_2^+, O_2^+, O, RNS, H_2O_2, NO_2, NO_3, N_2, O, H, free radicals	Gliding arc discharge	[23]
	Ar, O_2, N_2, O_2^+, O_2^-, O, O_3, N_2^+, NO, He, He^+, OH, RNS, ROS, N, ions, NH_3, H_2, O_2, NO_x, He-, He_2^+, NO_2^-, CN^-, NH, O_2, ions, free radicals	Microwave discharge	[21]
Vacuum-ultraviolet (VUV) and ultraviolet (UV) radiations for chemical modification including microbial deactivation	UV radiation and VUV	DBD discharge	[24]
		RF discharge	[20]
		Gliding arc discharge	[23]
		Microwave discharge	[21]
Energetic neutrals for physicochemical modification	Energetic N_2	Glow discharge	[6,7]

Even though the results of CPFP studies are highly promising, CPFP suffers from the following two major drawbacks in commercial applications [3]:

i) High processing gas cost

ii) Low energy efficiency of plasma sources

The use of gases such as helium, hydrogen, argon, neon, oxygen, pure nitrogen, etc., as the processing gas for the commercial application of CPFP turns out to be highly expensive [3]. Though the cost of pure nitrogen as the processing gas is estimated to be the minimum among the above-mentioned gases, the cost of N_2-processed food will be still beyond the affordability of the major portion of the population. In addition, most plasma sources used for CPFP have an energy efficiency of less than 10% of the total electrical power consumed. These two are the main challenges in the commercial application of CPFP.

To overcome these two challenges, we proposed the use of air in place of nitrogen as the processing gas, hence eliminating the processing gas cost completely. As air contains 78% N_2, accordingly we proposed that the charge exchange collision (CXC) between N_2^+ and N_2 may be utilized for the selective extraction of active species to enhance the energy efficiency of CPFP drastically. In the following section, the theoretical model for generating active species in glow discharge plasma is discussed.

3. Energetic N_2 and N_2^+ generation using CXC model

As listed in **Table 1**, the active species desired for physicochemical modification in CPFP are energetic species. The most commonly known energetic species are the ions of the processing gas. However, in the case of nitrogen as the processing gas, energetic N_2 can be also generated. The role of CXC in the velocity distribution of N_2 and N_2^+ inside a cathode sheath was investigated in detail in Suraj and Mukherjee's report [6]. The most interesting fact observed was that for DC glow discharge plasma, 90% of electrical energy goes to energetic N_2 neutrals and, consequently, processes such as plasma nitriding are low energy efficient. This leads to the concept that if energetic N_2 is itself used as an active species for physicochemical modification, then there is a possibility to overcome the second limitation of the low energy efficiency of CPFP. In this section, we discuss in detail how to generate energetic N_2 and N_2^+ with specific energy using CXC.

The one-dimensional model for CXC between N_2 and N_2^+ and the experimental arrangement for nitrogen DC glow discharge plasma is shown in **Figure 1**. The experimental plasma system for the treatment is shown in **Figure 1(a)**. In this figure, the components are as follows: (1) pressure gauge, (2) vacuum chamber, (3) connection to the mesh cathode (4) viewport, (5) SS mesh (acting as a transparent cathode to energetic N_2), (6) sample holder, (7) needle valve, (8) gas cylinder, (9) load resistor, (10) sample, (11) plasma, (12) power supply, and (13) rotary pump. The sample kept under the transparent electrode is treated by the species extracted from the plasma. The magnified view of the transparent cathode's region of the CXC model is shown in **Figure 1(b)**: (14) plasma cathode sheath boundary, (15) plasma ion sheath region, (16) N_2^+ ions from the plasma entering the sheath, (17) acceleration of N_2^+ ions inside the sheath, (18) energetic N_2^+ ions after gaining energy, (19) CXC between N_2 and N_2^+, (20) background N_2 neutrals, (21) energetic N_2 neutrals (generated when

energetic N_2^+ ions capture electrons via CXC), and (22) energetic N_2 neutrals striking the crossings of the SS mesh electrode, which is transparent to N_2 neutrals, to reach the bulk of the sample. It shows that when a negative potential V_0 is applied on the cathode positioned at $X = 0$, the applied voltage is entirely screened by the plasma within the cathode ion sheath with sheath thickness of $X = S$. Thus, $V_{X=0} = -V_0$ and $V_{X=S} = 0$. For low-pressure discharge, the N_2^+ ions entering the sheath reach the cathode's surface without undergoing any collision with the background gas molecules of N_2. In other words, the sheath thickness (S) is smaller than the mean free path (λ) for CXC, i.e., $S \ll 10\lambda$. At low pressures, when the sheath is collisionless, N_2^+ ions strike the cathode with an energy of $\frac{1}{2}mv^2 = eV_0$. Thus, the maximum velocity of ions striking the cathode is $v = u_m = (2eV_0/m_i)^{1/2}$. However, as shown in the figure, the sheath becomes collisional at higher pressures, where N_2^+ ions undergo CXC with the background N_2 neutrals, which are at rest. The background N_2 neutrals become N_2^+ ions, and the accelerating N_2^+ ions become N_2 neutrals. The newly born N_2^+ ions have no kinetic energy, but the newly born N_2 neutrals retain the energy of the N_2^+ ions. The energetic N_2 neutrals travel towards the electrode without further collision, as the cross-sections for neutral-neutral collision are significantly low [28]. The energetic N_2 neutrals can cross a mesh electrode with finite transparency, as shown in **Figure 1(b)**. The energetic N_2 neutrals are extracted using this simple technique utilized for treatment. The newly born N_2^+ ions begin to accelerate towards the electrode and further undergo charge exchange collision with the background neutrals. The position of the CXC, where the newly born N_2^+ ions have zero velocity, is referred to as X_0. Since the potential gradient is strong near the cathode's surface and weak near the plasma sheath boundary, the ions gain different velocities in different regions of the sheath.

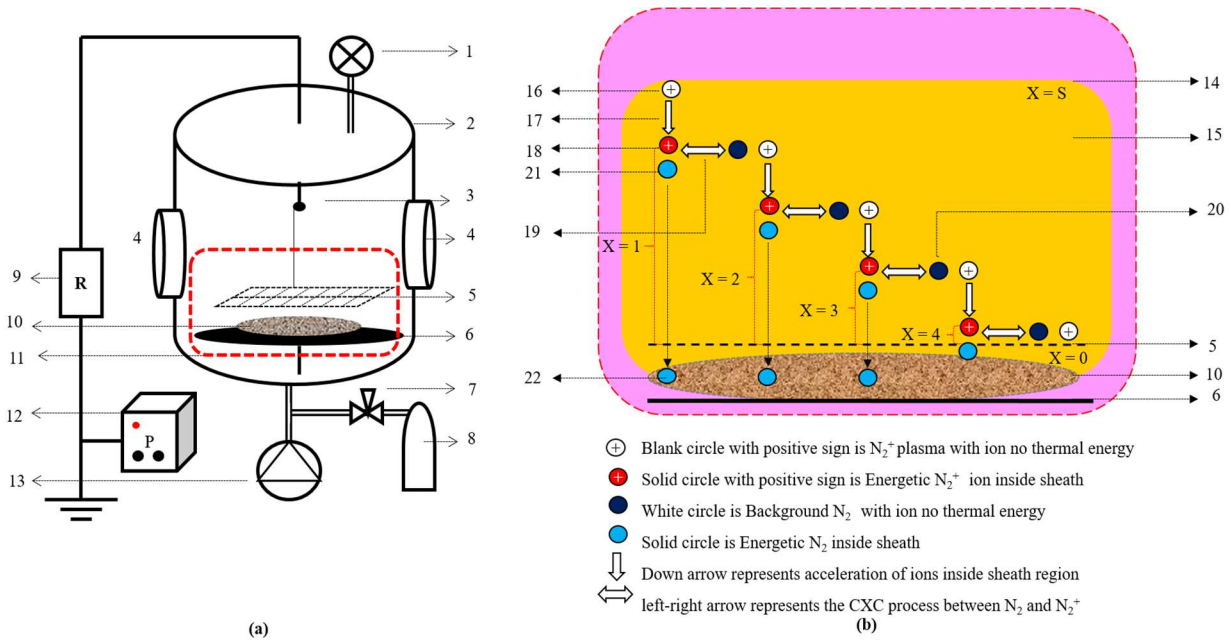

Figure 1. (a) Experimental plasma system used for treatment of samples. **(b)** Magnified view of transparent cathode's region.

It is a well-known fact that sheath thickness depends on collisions. When sheath thickness (S) is significantly larger than the mean free path (λ), the sheath is collisionless ($10S\sim\lambda$). Child's law expresses the potential profile of a collisionless sheath. For a fully collisional sheath, i.e., when $S\sim10\lambda$, the potential profile is expressed by the collisional law [6]. Using this knowledge, the energy values of the energetic N_2 and N_2^+ ions cannot be estimated in an intermediate/partially collisional sheath, where sheath thickness is defined as $0.1\lambda \leq S \leq 10\lambda$, and the potential profile needs to be estimated numerically. This intermediate region holds the key for the selective extraction of N_2^+ and energetic N_2 with specific energies, which is the crux of the present investigation.

The potential profile inside a sheath can be generalized in the form of a power law, as given below [6]:

$$V_0 = \frac{V_X}{[(S-X)^b/S^b]} \tag{1}$$

where V_0 is the applied voltage on the cathode, b is the power exponent, X is the position inside the cathode sheath, V_X is the potential at position X, and S is the sheath thickness. The power exponent reduces to $b\approx4/3$ for $\lambda/10 \approx S$; hence, when S is one-tenth of λ, the sheath becomes collisionless. On the other hand, the power exponent reduces to $b\approx5/3$ for $10\lambda \approx S$; hence, when S is ten times larger than λ, the sheath becomes fully collisional. The thickness of a collisionless sheath is significantly larger than that of a fully collisional sheath [28]. In the partially collisional region, i.e., $0.1\lambda \geq S \geq 10\lambda$, b can be evaluated numerically from the known applied cathode voltage if the electric field (V_0') and electric field gradient (V_0'') at the cathode's surface are known. These values are obtained for a typical experimental condition by numerically solving the fluid equations of a coupled plasma [6]. In the presence of CXC between ions and the background, the governing equations are:

$$\partial_X(1/2\, v_i^2) = -e/m_i \partial_X V_X - n_n \sigma v_i^2 \tag{2}$$

$$\partial_X^2(V_X) = -en_0/\varepsilon\, [v_0/v_i - exp(\frac{eV}{k_B T_e})] \tag{3}$$

where $\partial_X = \partial/\partial X$, v_i is the ion velocity inside the cathode sheath, m_i is the ion mass, k_B is the Boltzmann constant, and T_e is the electron's temperature. These two generalized equations describe a one-dimensional collisional plasma sheath and are a combination of all four governing plasma equations [28]. In this study, the values used for the initial condition at the plasma-sheath boundary were $V \approx 0.01\ volts$ and $V' \approx 0.01\ volts/m$, and hence the equations can be solved numerically to obtain the electric field (V_0') and its spatial derivative (V_0'') at the cathode's surface from the applied cathode voltage and the known plasma density [6]. The values of V_0' and V_0'' are obtained numerically by solving Equation (2) and Equation (3), followed by the evaluation of b and S using the relationship of $b = 1/\left[1 - V_0 V_0^{"}/(V_0')^2\right]$ and $S = bV_0/V_0'$. For known values of S and b, the normalized ion velocity distribution at the electrode is expressed as [6,29]:

$$f_i(u,z) = 2\left[\frac{(uS^b)}{\left\{\lambda b u^2 z^{b-1}\left(1-\frac{u^2 S}{u^2 z^b}\right)^{b-1/b}\right\}}\right] exp\left[-\left(\frac{z}{\lambda}\right)\left\{1-\left(1-\frac{u^2 S}{u^2 z^b}\right)^{b-1/b}\right\}\right] \tag{4}$$

where $z = S - X_0$ is the position of CXC inside the cathode sheath, u is the ion

velocity, and $u_m = (2eV_0/m_i)^{1/2}$ is the maximum ion velocity at the cathode. Energetic N_2 neutrals' velocity can be obtained by multiplying $f_i(u,z)$ with the probability of CXC that the accelerating ions undergo when traversing distance *dz* on the way to the cathode, and the integral of this product over sheath thickness *S* gives the velocity distribution of energetic N_2 neutrals:

$$f_n(u, z = S) = \int_0^S f_i(u,z).\frac{dz}{\lambda} \quad (5)$$

where dz/λ is the probability for ions undergoing CXC within element *dz*. This model is briefly explained in the following sections.

4. Discussion

The values of power exponent *b* and sheath thickness *S* are obtained from an experimental condition using Equations (1–3), while the velocity distributions of N_2^+ and N_2 at the cathode's surface are obtained numerically using Equations (4) and (5), respectively. For a typical CPFP condition for the CXC between N_2^+ and N_2, with cathode voltages of $V_0 = -1\ kV$ and $V_0 = -5\ kV$, plasma density of n_e=1×10^{16} m^{-3}, plasma temperature of $T_e = 1.0\ eV$, and cross-section of 4×10^{-19} m^2, the value of sheath thickness *S*, mean free path λ, and power exponent *b* can be obtained numerically for different pressures, as listed in **Table 2**. At pressure of 1×10^{-4} mbar, $\lambda = 1010.1$ mm, and $S = 5.2$ mm and 0.2 mm at V_0 of –1 kV and –5 kV, respectively, the sheath is collisionless, since $b = 1.34 \cong 4/3$, and hence the potential profile is expressed by Child's law. The N_2^+ ions entering the plasma sheath can reach the surface of the negatively biased electrode without suffering any collision, with energy of $^1/_2\ mu_m^2 \sim eV_0 \cong 1$ keV.

Keeping all operating parameters fixed and increasing the pressure from 0.0001 mbar to 0.1 mbar, i.e., from a collisionless to fully collisional sheath, various parameters can be numerically estimated, as listed in **Table 2**. **Figure 2(a)** and **Figure 2(c)** show the f_i and f_n distributions, respectively, resulting from the CXC at the operating pressure of 0.01 mbar. Though the sheath thickness is larger than the mean free path ($S = 4.56$ mm and 4.7 mm, $\lambda = 10.1$ mm), there is a finite probability that the N_2^+ ions undergo CXC before reaching the cathode. However, many reach the cathode without undergoing CXC. Therefore, the sheath is fully collisional. As seen in **Figure 2(a)**, the collisionless ions cause a sharp peak in the velocity distributions of N_2^+ ions at u_m of 8.30×10^4 m/s and 18.50×10^4 m/s at V_0 of −1.0 kV and −5.0 kV, respectively. From **Table 2**, the mean energy values of N_2^+ ions and energetic N_2 obtained at pressure of 0.01 mbar are 0.56 keV and 1.33 keV, respectively, at cathode voltage of −1.0 kV and are 0.22 keV and 1.17 keV, respectively, at cathode voltage of −5.0 kV. This shows that most of the N_2^+ ions undergo CXC near the cathode after accelerating in a larger portion of the sheath.

Table 2. Estimated values of mean free path (λ), sheath thickness (S), power exponent (b), mean velocity of N_2^+ (u_i), mean velocity of energetic N_2 (u_n), energy of N_2^+ ions (E_i), average energy of neutral N_2 (E_n), and number of energetic N_2 neutrals generated per ion (N_N) for typical glow discharge plasma at cathode voltages of –1.0kV and –5.0 kV.

V_0 (kV)	P (mbar)	λ (mm)	S (mm)	b	Velocity distribution ($\times 10^4$ m/s, $u_i(max) = u_m = (2eV_0/m_i)^{1/2}$)		Mean energy (keV)		N_N
					u_i	u_n	E_i	E_n	
−1.0	0.0001	1010.10	5.20	1.34	8.30	-	1.0	-	NIL
	0.001	101.0	5.14	1.35	8.30	-	1.0	-	NIL
	0.01	10.1	4.56	1.44	6.37	4.04	0.56	0.22	2.02
	0.1	1.01	1.86	1.62	2.20	1.50	0.10	0.07	13.56
−5.0	0.0001	1010.10	0.2	1.34	18.50	-	5.0	-	NIL
	0.001	101.0	9.5	1.37	18.50	-	5.0	-	NIL
	0.01	10.1	4.7	1.55	8.10	5.70	1.33	1.17	5.70
	0.1	1.01	2.6	1.65	3.00	1.90	0.20	0.11	34.35

Note: N_2^+ ions reach the cathode surface with maximum velocity (u_m), e is the electronic charge, Vo is the electrode potential and m_i is the ion mass.

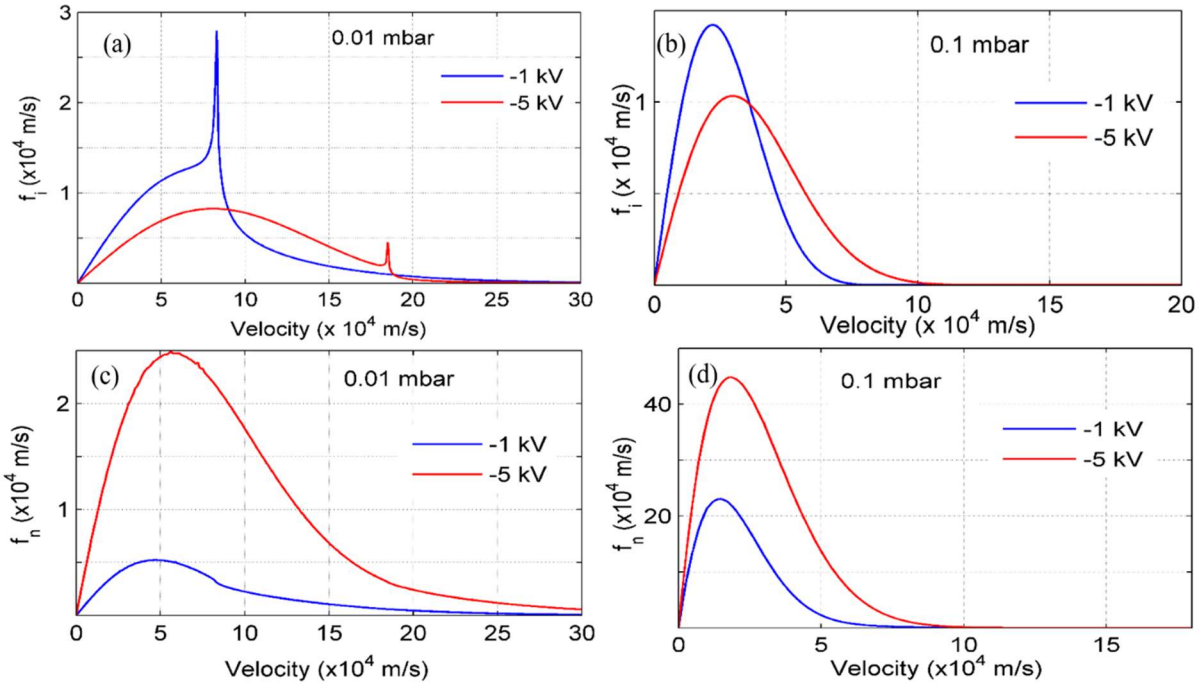

Figure 2. Distributions of f_i at cathode voltages of −1.0 kV and −5.0 kV: **(a)** 0.01 mbar and **(b)** 0.1 mbar. Distributions of f_n at cathode voltages of −1.0 kV and −5.0 kV: **(c)** 0.01 mbar and **(d)** 0.1 mbar.

The ions with higher velocity than u_m in the graphs are ions that enter the plasma sheath boundary [28]. The average velocity of energetic neutrals is always less than the average velocity of ions generated inside a cathode sheath. However, a few ions with higher velocity than u_m is possible, which accounts for the acceleration in the presheath region. It is interesting to note that at pressure of 0.01 mbar and cathode

voltage of −1.0 kV, the average velocity of the ions (V_i) is 8.30×10^4 m/s, while at cathode voltage of −5.0 kV, the average velocity is 18.50×10^4 m/s which is higher. This is because the sheath becomes more collisional at −5.0 kV. For every 100 ions entering the sheath, 202 and 570 energetic neutrals are produced via CXC at −1.0 kV and −5.0 kV, respectively.

The increase in pressure from 0.01 to 0.1 mbar decreases the mean free path (λ) from 10.1 mm to 1.01 mm, and sheath thicknesses reduce from 4.56 mm to 1.86 mm and from 4.7 mm to 2.6 mm for cathode voltages of −1.0 and −5.0 kV, respectively. Thus, the sheath becomes fully collisional at 0.1 mbar, and therefore the peaks of f_i and f_n shift towards a lower velocity. For this case, for every 100 ions entering the sheath on the way to the cathode's surface, 1356 and 3435 energetic neutrals are generated via CXC at cathode voltages of −1.0 kV and −5.0 kV, respectively.

Figure 2(a) and **Figure 2(c)** show the f_n and f_i distributions at 0.01 mbar, respectively, with the fixed scale of the x-axis (×10^4 m/s) and y-axis (×10^{-4}). In contrast, **Figure 2(b)** and **Figure 2(d)** show the f_n and f_i distributions, respectively, at pressure of 0.1 mbar. The same distribution trends at 0.01 mbar are maintained at 0.1 mbar, where the number of energetic neutrals generated per ion increases and the peaks of f_i and f_n further shift towards a lower velocity. The mean energy values of ions and neutrals reaching the cathode decrease with increased pressure, as the number of energetic N_2 increases. At 0.1 mbar, the mean energy values of N_2^+ ions and energetic N_2 reaching the cathode are 0.10 keV and 0.07 keV at −1.0 kV, respectively, and 0.20 keV and 0.11 keV at −5.0 kV, respectively.

Using CXC, among the four dominant species in nitrogen glow discharge plasma, any desired species can be selectively extracted by controlling the operating parameters. In the case of energetic nitrogen molecular ions (N_2^+), the operating parameters in **Table 2** can be used. As estimated from the method discussed above, at pressure = 1×10^{-4} mbar, with $S = 5.20$ mm and 0.2 mm at V_0 of –1 kV and –5 kV, respectively, the mean free path for charge exchange collision is $\lambda = 1010.1$ mm. Therefore, molecular nitrogen ions (N_2^+) reach the cathode without suffering collisions, as $\lambda \gg S$, with an energy equivalent to the applied voltage on the cathode, i.e., 1 keV and 5 keV. Therefore, at low pressures and with a cathode mesh with a large gap (l) between the electrode wires, such that $l \ll S$, as well as a high cathode grid transparency of $\sim 90\%$, the most dominant species extracted are N_2^+ ions. On the other hand, for energetic N_2, at the increased pressure of 0.01 mbar, with $S = 4.56$ mm and 4.7 mm at V_0 of –1 kV and –5 kV, respectively, the mean free path for charge exchange collision is $\lambda = 10.1$ mm. Therefore, each molecular nitrogen ion (N_2^+) will undergo at least one CXC before reaching the cathode, as $\lambda \sim S$. Each N_2^+ ion reaches the cathode with an energetic N_2 neutral at the cost of its energy, which reduces from 1 keV and 5 keV for the collisionless sheath to ~ 0.22 keV and ~ 1.17 keV at V_0 of –1 kV and –5 kV, respectively. With a further increase of pressure to 0.1 mbar, each N_2^+ ion generates 10 energetic N_2. Thus, with every ion, 10 neutrals reach the cathode. For an operating condition such that $\lambda \sim S$ and with a high cathode grid transparency of $\sim 50\%$, the cathode grid obstructs the ions. Most of the energetic N_2 are extracted at the cathode. Furthermore, for nitrogen DC glow discharge plasma, the main emission lines observed are N_2^+ ($B^2\sum_u^+ \rightarrow X^2\sum_g^+$) at 391.4 nm, 427.8 nm, 470.9 nm,

and 522.8 nm; N_2^+ ($A^2\prod_u \rightarrow X^2\sum_g^+$) at 782.5nm; N_2 ($C^3\prod_u \rightarrow B^3\prod_g$) at 337.1 nm, 357.6 nm, 375.5 nm, and 380.5 nm; and N_2 ($B^3\prod_g \rightarrow A^3\prod_u^+$) at 537.2–804.8 nm. Additional oxygen and hydrogen lines are observed for air plasma at 777 nm, 844 nm, 656.2 nm, and 486.1 nm for N_2-H_2 discharge plasma. Under a relatively higher-pressure condition, such as 10 mbar, and at cathode voltage = −500 V, the mean free path is $\lambda = 1.01 \times 10^{-2}$ mm and the sheath thickness is $S = 3.38$ mm. The energy values of N_2^+ and N_2 at the cathode's surface are as low as $\sim$ 2.0 eV and insignificant for the treatment. However, the intensity of N_2^+ and N_2 emission lines increases by several factors. Under these conditions, radiation dominates, and the energy of plasma species reaching the cathode is relatively low. Nevertheless, these energy radiations (391.4 nm) have negligible effects on the process [3,11,12]. The addition of an appropriate gas in a small fraction may result in ultra-violet radiation suitable for an effective treatment of a sample. Nitrogen discharge plasma can generate reactive atomic species (nascent atomic nitrogen N) under typical operating conditions. At low pressures, such as at pressure of 1×10^{-4} mbar, with $S = 5.2$ mm and 0.2 mm at V_0 of –1 kV and –5 kV, respectively, and $\lambda = 1010.1$ mm ($\lambda \gg S$), N_2^+ ions have an energy equivalent to the applied cathode voltage (1.0 keV to 5.0 keV) to reach the cathode without collisions. For a low-transparency cathode grid of ~20%–30%, most ions, with energy of $\sim$ 1.0 to 5.0 keV, strike the cathode grid wires and dissociate into nascent atomic nitrogen (N). Under these operating conditions, nascent atomic nitrogen N is the dominant species at the cathode's surface.

5. Significance of CXC on active species generation

From the numerical modeling of CXC between N_2 and N_2^+ for nitrogen DC glow discharge plasma, the velocity distribution of each has been estimated via two controlling parameters, namely applied voltage and operating pressure. The most significant results of the model are the following:

i) N_2^+ ions are generated as the most dominant active species when the sheath is collisionless, i.e., when the collision mean free path is larger than the sheath thickness (i.e., $\lambda \gg S$) and the value of power exponent b is ~1.35, where the ions gain energy equivalent to the applied voltage.

ii) Energetic N_2 ions are generated as the most dominant active species when the sheath is fully collisional, i.e., when the sheath thickness is larger than the collision mean free path (i.e., $S \gg \lambda$) and the value of power exponent b is ~1.66, as the energy of N_2 neutrals depends on collisions.

iii) Highly chemically active nascent atomic nitrogen N can be generated when N_2^+ ions with sufficiently high energy, as generated under the condition of a collisionless sheath, strike the cathode. Therefore, when the transparency of the mesh grid shown in **Figure 1** is less than 30%, all energetic N_2^+ ions strike the mesh cathode and dissociate.

iv) Both energetic N_2 and N_2^+ can be generated simultaneously when the sheath is partially collisional (i.e., $S \sim \lambda$).

v) The energy and number of the active species generated can be controlled by the parameters of operating pressure and applied cathode voltage.

6. Experimental demonstration

The principle was experimentally demonstrated for the modification of physicochemical and rheological properties of kittul starch, talipot starch, and corn flour by energetic N_2 neutrals extracted from glow discharge air plasma [7,8,9,30,31]. Interestingly, as air was proposed as the processing gas and since it contains ~78% N_2, the model developed for pure nitrogen was considered as applicable under approximation. Therefore, we demonstrated that it is possible to extract energetic N_2 and N_2^+ ions with specific energies from air plasma for physicochemical modification for CPFP.

The morphological characteristics of untreated and plasma-treated kithul starch, talipot starch, and corn flour samples are shown in **Figure 3**. At pressures of 0.2 and 0.5 mbar and cathode bias of −500 V, nearly 80% of the ions' energy went to energetic N_2 neutrals and was utilized to modify its physicochemical properties [7,9,30,31]. With the limited transparency of the mesh grid at 65%, the estimated energy efficiency of the process was more than 40% (more than 40% of total electrical power used in the discharge is dumped to the samples under treatment by energetic N_2 neutrals).

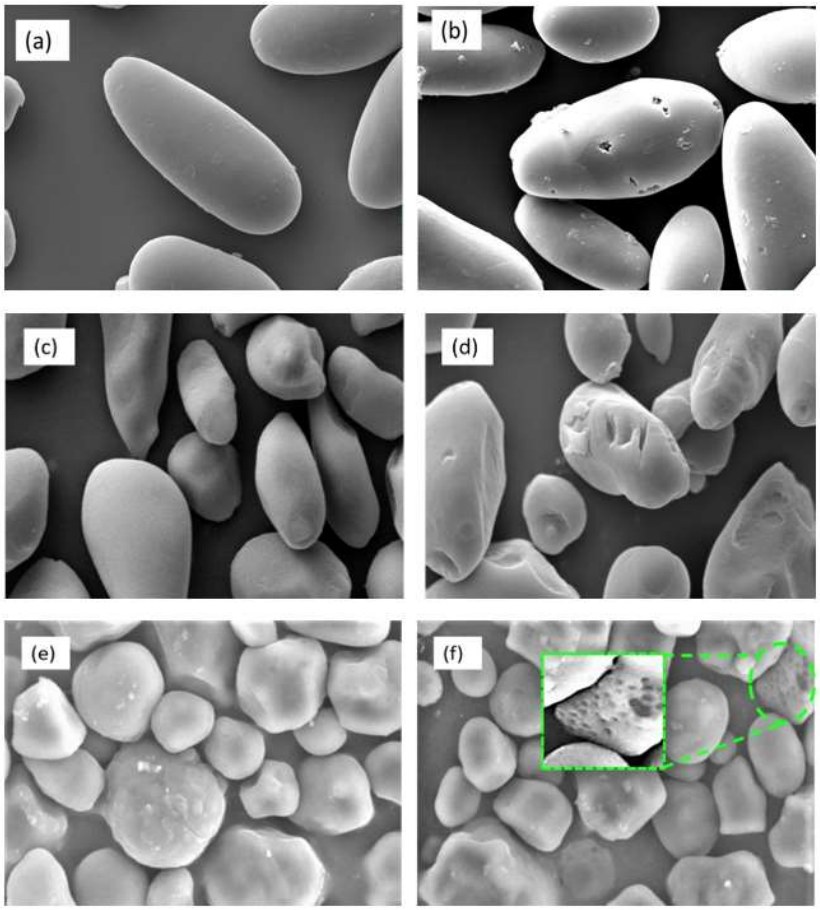

Figure 3. Scanning electron microscopy images of **(a)** untreated kithul starch, **(b)** plasma-treated kithul starch [7], **(c)** untreated talipot starch, **(d)** plasma-treated talipot starch [9], **(e)** untreated corn flour, and **(f)** plasma-treated corn flour [30].

7. Conclusion

In conclusion, this work presents how the CXC between N_2 and N_2^+ inside a cathode sheath can be utilized for the selective generation of desired active species under the glow discharge plasma condition. The results obtained from this analysis show that by tuning the operating parameters, one can get the desired active species with the desired energy range for the processing of a wide range of food products. Moreover, as an added advantage, since air contains 78% nitrogen, it can be used to minimize the processing gas cost, and the treatment by energetic N_2 neutrals can drastically improve the energy efficiency of CPFP devices. This work can be extended to pulsed DC discharge, different gaseous mixtures for a wide range of operating pressures, and different discharge voltages. Thus, the present investigation may provide a new direction to overcome the limitations of CPFP and make it viable for all commercial applications.

Ethical approval: Not Applicable.

Data Availability: Data available within the article.

Author contributions: SKS: overall research supervision, conceptualization, visualization, innovations, writing, data curation, and editing. MP: experiment, validation, writing, theoretical and numerical investigation, review, data curation, and analysis of data. MP and AS: numerical estimations, and original draft writing. BM: formal analysis and editing. All authors have reviewed and approved the final version of the manuscript.

Funding: Not Applicable.

Conflict of interest: The authors declare no conflict of interest.

References

1. Thirumdas R, Sarangapani C, Annapure US. Cold Plasma: A novel Non-Thermal Technology for Food Processing. Food Biophysics. 2014; 10(1): 1-11. doi: 10.1007/s11483-014-9382-z
2. Boeuf JP. Plasma display panels: physics, recent developments and key issues. Journal of Physics D: Applied Physics. 2003; 36(6): R53-R79. doi: 10.1088/0022-3727/36/6/201
3. Niemira BA. Cold Plasma Decontamination of Foods. Annual Review of Food Science and Technology. 2012; 3(1): 125-142. doi: 10.1146/annurev-food-022811-101132
4. López M, Calvo T, Prieto M, et al. A Review on Non-thermal Atmospheric Plasma for Food Preservation: Mode of Action, Determinants of Effectiveness, and Applications. Frontiers in Microbiology. 2019; 10. doi: 10.3389/fmicb.2019.00622
5. Pankaj S, Wan Z, Keener K. Effects of Cold Plasma on Food Quality: A Review. Foods. 2018; 7(1): 4. doi: 10.3390/foods7010004
6. Suraj KS, Mukherjee S. Power balance at cathode in glow discharges. Physics of Plasmas. 2005; 12(11). doi: 10.1063/1.2127929
7. Sudheesh C, Sunooj KV, Sinha SK, et al. Impact of energetic neutral nitrogen atoms created by glow discharge air plasma on the physico-chemical and rheological properties of kithul starch. Food Chemistry. 2019; 294: 194-202. doi: 10.1016/j.foodchem.2019.05.067
8. Sudheesh C, Sunooj KV, Sasidharan A, et al. Energetic neutral N_2 atoms treatment on the kithul (*Caryota urens*) starch biodegradable film: Physico-chemical characterization. Food Hydrocolloids. 2020; 103: 105650. doi: 10.1016/j.foodhyd.2020.105650

9. Navaf M, Sunooj KV, Aaliya B, et al. Impact of Low-Pressure Argon Plasma on Structural, Thermal, and Rheological Properties of *Corypha umbraculifera* L. Starch: A Non-Conventional Source of Stem Pith Starch. Starch - Stärke. 2022; 75(1-2). doi: 10.1002/star.202200165
10. Raizer YPP. Gas Discharge Physics. Springer; 1997.
11. Chapman B. Glow Discharge Processes: Sputtering and Plasma Etching. John Wiley & Sons; 1980.
12. Lieberman MA, Lichtenberg AJ. Principle of Plasma Discharges and Material Processing. John Wiley & Sons; 1994.
13. Moisan M, Barbeau J, Crevier MC, et al. Plasma sterilization. Methods and mechanisms. Pure and Applied Chemistry. 2002; 74(3): 349-358. doi: 10.1351/pac200274030349
14. Mir SA, Shah MA, Mir MM. Understanding the Role of Plasma Technology in Food Industry. Food and Bioprocess Technology. 2016; 9(5): 734-750. doi: 10.1007/s11947-016-1699-9
15. Chizoba Ekezie FG, Sun DW, Cheng JH. A review on recent advances in cold plasma technology for the food industry: Current applications and future trends. Trends in Food Science & Technology. 2017; 69: 46-58. doi: 10.1016/j.tifs.2017.08.007
16. Muhammad AI, Liao X, Cullen PJ, et al. Effects of Nonthermal Plasma Technology on Functional Food Components. Comprehensive Reviews in Food Science and Food Safety. 2018; 17(5): 1379-1394. doi: 10.1111/1541-4337.12379
17. Prakash R, Hossain AM, Pal UN, et al. Dielectric Barrier Discharge based Mercury-free plasma UV-lamp for efficient water disinfection. Scientific Reports. 2017; 7(1). doi: 10.1038/s41598-017-17455-2
18. Grzegorzewski F, Zietz M, Rohn S, et al. Modification of polyphenols and cuticular surface lipids of Kale (*B. oleracea* convar. *sabellica*) with non-thermal oxygen plasma gaseous species. In: Proceedings of the 11th International Congress on Engineering and Food; 22–26 May 2011; Athens, Greece.
19. Bursać Kovačević D, Gajdoš Kljusurić J, Putnik P, et al. Stability of polyphenols in chokeberry juice treated with gas phase plasma. Food Chemistry. 2016; 212: 323-331. doi: 10.1016/j.foodchem.2016.05.192
20. Lassen KS, Nordby B, Grün R. The dependence of the sporicidal effects on the power and pressure of RF-generated plasma processes. Journal of Biomedical Materials Research Part B: Applied Biomaterials. 2005; 74B(1): 553-559. doi: 10.1002/jbm.b.30239
21. Lee KY, Joo Park B, Hee Lee D, et al. Sterilization of *Escherichia coli* and MRSA using microwave-induced argon plasma at atmospheric pressure. Surface and Coatings Technology. 2005; 193(1-3): 35-38. doi: 10.1016/j.surfcoat.2004.07.034
22. Lu X, Ye T, Cao Y, et al. The roles of the various plasma agents in the inactivation of bacteria. Journal of Applied Physics. 2008; 104(5). doi: 10.1063/1.2977674
23. Niemira BA, Sites J. Cold Plasma Inactivates *Salmonella* Stanley and *Escherichia coli* O157: H7 Inoculated on Golden Delicious Apples. Journal of Food Protection. 2008; 71(7): 1357-1365. doi: 10.4315/0362-028x-71.7.1357
24. Lee KH, Kim HJ, Woo KS, et al. Evaluation of cold plasma treatments for improved microbial and physicochemical qualities of brown rice. LWT. 2016; 73: 442-447. doi: 10.1016/j.lwt.2016.06.055
25. Ulbin-Figlewicz N, Brychcy E, Jarmoluk A. Effect of low-pressure cold plasma on surface microflora of meat and quality attributes. Journal of Food Science and Technology. 2013; 52(2): 1228-1232. doi: 10.1007/s13197-013-1108-6
26. Dixon D, J. Meenan B. Atmospheric Dielectric Barrier Discharge Treatments of Polyethylene, Polypropylene, Polystyrene and Poly(ethylene terephthalate) for Enhanced Adhesion. Journal of Adhesion Science and Technology. 2012; 26(20-21): 2325-2337. doi: 10.1163/156856111x599481
27. Perumal M. Study of DC Glow Discharge Plasma for Selective Generation Active Species for Cold Plasma Processing [PhD thesis]. Pondicherry University; 2022.
28. Suraj KS, Mukherjee S. Effect of ion neutral collisions on the ion and neutral velocity distribution on negatively biased electrodes. Surface and Coatings Technology. 2005; 196(1-3): 267-270. doi: 10.1016/j.surfcoat.2004.08.101
29. Mukherjee S. Neutral velocity distribution at a negatively biased electrode in a collisional ion sheath. Physics of Plasmas. 2001; 8(1): 364-367. doi: 10.1063/1.1327619
30. Perumal M, Saravanan A, Sunooj KV, et al. Effect on Physical and Thermal Properties of Corn Starch Treated by Energetic N_2 Extracted From Glow Discharge Plasma. IEEE Transactions on Plasma Science. 2022; 50(4): 1122-1127. doi: 10.1109/tps.2022.3155663
31. Perumal M, Saravanan A, Kommuguri SL, et al. Extraction of Energetic N_2 Neutrals for Efficient Plasma Food Processing of Finger Millet Flour. Plasma Chemistry and Plasma Processing. 2023; 44(1): 471-485. doi: 10.1007/s11090-023-10383-2